ACS OMEGA

http://pubs.acs.org/journal/acsodf

Article

Effect of the Dispersion Process and Nanoparticle Quality on Chemical Sensing Performance

Elias Mansour,[§] Shay Sherbo,[§] Walaa Saliba, Viki Kloper, and Hossam Haick*

Cite This: *ACS Omega* 2022, 7, 22484−22491

Read Online

ACCESS | Metrics & More | Article Recommendations | Supporting Information

ABSTRACT: On the surface of chemiresistive films, the scarce heterogeneity of a molecularly capped gold nanoparticle (MCGNP) colloidal dispersion and uneven evaporation of the MCGNP-contained drying drop applied to this surface are among the main factors that affect reproducibility, and repeatable fabrication of thin films of MCGNPs. This article shows that an increase in reproducibility and repeatability is possible using a dispersant and a surfactant during the deposition and annealing processes of the MCGNP. The results show higher sensitivity and accuracy of the sensors for the detection of volatile organic compounds in air and an increased limit of detection. These simple and practical additions might serve as a launching pad for fabrication of other types of thin-film-based sensors.

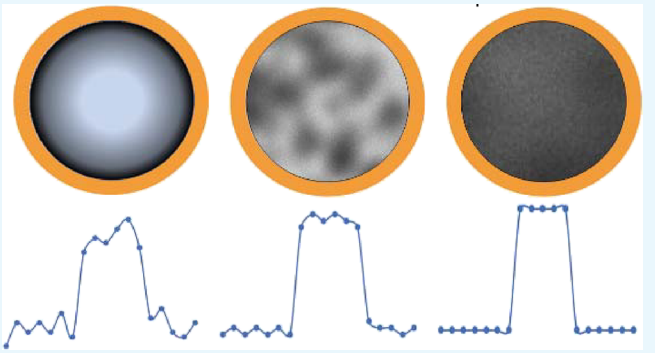

INTRODUCTION

Sensing volatile organic compounds (VOCs) using chemical sensors based on thin films of molecularly capped metallic nanoparticles (MCNPs) is a powerful potential technology that can be used in disease diagnosis,[1−5] monitoring of outdoor and indoor air,[6−8] and for the quality control of food products.[9−11] There are many reasons why it is advantageous to design chemical assays around these nanomaterials, but there are three that are noteworthy here:[12−15] (1) the versatility of the composition of the nanomaterial itself, (2) the ability to vary the nanomaterial size and/or shape and, therefore, the surface-to-volume ratio, and (3) the ability to prepare films of nanomaterials that have controllable porous properties,[16−18] controllable mass transport (e.g., via diffusion), and controllable permittivity of the film.

The production of MCNP-based chemiresistors starts with the synthesis of nanoparticles with specific organic ligands, using two-phase,[19] one-phase,[20] and water-soluble[21,22] approaches. This is followed by the assembly of thin films made of MCNPs between adjacent microelectrodes. There are several deposition methods on microelectrodes such as drop-casting,[23] layer-by-layer deposition,[24,25] spin coating,[26] spraying,[27] etc. However, most fabrication techniques lack reproducibility and repeatability mainly due to the uneven evaporation of the MCNP-contained drying drop applied on the surface.[28,29] This phenomenon occurs despite strict control over the printing volume, particle size, temperature, relative humidity, and the surrounding gas atmosphere.[29−32] The uneven evaporation forms coffee ring-like structures characterized by above average particle density inside the ring and a lesser amount of particles at the center of the surface of interest.[33]

One approach for reducing the percentage of irregularity in the sensing film relies on the addition of a dipolar aprotic and high-boiling-point solvent to the water-based MCNP solution.[31,34,35] This approach reduces the pinning effect of the contact line with the substrate and therefore the irregularities. However, water-based solutions are less suitable in the production of functioning MCNP-based chemiresistors. Other studies have shown that the addition of surfactants[36] and different organic solvents with different vapor pressures[37] to the MCNP solution and the application of electrowetting[38] or surface acoustic waves,[39] can lead to the production of fully homogeneous disk-shaped patterns. Still, the cost efficiency of sensing films using these approaches remains relatively low.

Here, we describe a method of increasing the stability and reproducibility of the chemical sensors based on molecularly capped gold nanoparticles (MCGNPs), by utilizing a dispersant and a surfactant for the deposition of ligand-capped GNPs and removing them afterward. The sensor's performance was measured via exposure to different pure VOCs and compared with sensors produced in the standard method. The validity of the fabrication steps was further confirmed using

Received: March 19, 2022
Accepted: June 6, 2022
Published: June 17, 2022

attenuated total reflectance (ATR) and scanning electron microscopy (SEM). The sensor performance was further enhanced using bromide instead of more commonly used chloride as the precursor for MCGNP synthesis since it produces higher yields of MCGNPs without the agglomerated byproducts.[40] This finding was confirmed using transmission electron microscopy (TEM). The two processes were combined to provide a tunable sensor with superior properties.

METHODS

Sensor Synthesis and Fabrication. *tert*-Dodecanethiol (Sigma-Aldrich, 25103-58-6)-capped nanoparticles were synthesized using a modified Brust method with either $HAuCl_4 \cdot 3H_2O$ (Sigma-Aldrich, 16961-25-4) or $NaAuBr_4 \cdot 2H_2O$ (Alfa Aesar, 10378-49-1) as a precursor.[3,40] Nanoparticles in toluene were mixed with 0.05% Byk-3760 (BYK Chemie GmbH) and 1% Solsperse 75000 (Lubrizol) (final concentration) and drop-casted (0.4ul) on a microelectronic transducer that consisted of circular interdigitated gold electrodes deposited by an electron-beam evaporator TFDS-870 (Vacuum Systems & Technologies, Petah Tikva, Israel) on a piece of silicon wafer capped with 1 μm of thermal oxide (Silicon Quest International, Reno, Nevada). The outer diameter of the circular electrode area was 3 mm, and the gap between two adjacent electrodes and the width of these electrodes were both 20 μm.[41] The sensors were allowed to dry for 5 min and submerged in a washing solution (50% v/v ethyl acetate:ethanol) in an open glass chamber inside a hood. The sensors were then annealed using SVA (solvent vapor annealing) by putting the sensors in a closed chamber filled with heated chloroform at 30 °C for 2−16 h.[42]

Attenuated Total Reflectance (ATR). ATR was performed using a Bruker (V-70) Fourier transform infrared (FTIR) spectrometer with a PIKE single-reflection horizontal attenuated total reflectance (ATR) accessory in the range of 399−7496 cm^{-1} (actual working range of 500−4000 cm^{-1}) with a DTGS detector. The sample consisted of MCGNPs drop-casted on top of a cleaned silicon wafer.

Exposure Chamber. A gas exposure system was utilized to assess the fabricated sensor's performance. The system consisted of a stainless-steel chamber connected to a Keithley multimeter and a data acquisition system (model 2701 INTEGRA SERIES) to measure the sensors. The chamber had two vents each controlled by a digital valve, one connected to a vacuum pump (EDWARDS nXDS10i) and the other connected to the simulation gas system. The latter was a custom-made bubbler-controlled system composed of an MFC (mass flow controller), a switch, and a glass bubbler. The desired VOC was put in a liquid form into the bubbler, and the concentration was controlled by changing the nitrogen carrier flow. The concentration was calculated by first deriving the saturation pressure using the modified Riedel equation[43] and then converting it to "ppm" with the ratio between the flow in the bubbler and the carrier nitrogen flow. The valve controller system and the Keithley multimeter were both connected to a computer with a LabVIEW (2012, version 12.0f1) script that controlled both valves of the simulation gas and vacuum and recorded the signal. The workflow of the experiment included the following steps: (1) vacuum for stabilization, (2) exposure to nitrogen, (3) vacuum, (4) exposure to a certain concentration of the VOC, and (5) vacuum, and the last two steps (4 and 5) were repeated with the number of concentrations that were needed. The applied voltage for each sensor was 5 V.

Feature Extraction of Sensor Array Data. The output of the gas exposure system was a vector of the resistance change for each sensor (a maximum of 40 sensors can be measured at once in the chamber). Using this output, we extracted one representative feature, which was the difference between the middle of the response step and the vacuum baseline before the response, divided by the baseline. Several exposure tests were performed in the same experiment, and therefore, several values of the features were extracted for every exposure.

Sensor Imaging. Scanning electron microscopy (SEM) and transmission electron microscopy (TEM) were outsourced and done at the Technion Center for Electron Microscopy and Soft Matter. TEM was performed with an FEI Talos 200 keV TEM with a Schottky FEG electron source. SEM was performed by a Zeiss Ultra Plus high-resolution SEM equipped with a field emission gun. Micrographs were taken at a low acceleration voltage of 1 kV and a working distance of 5 mm.

RESULTS AND DISCUSSION

Experimental Design Scheme. MCGNPs were synthesized using gold precursors ($HAuCl_4 \cdot 3H_2O$ or $NaAuBr_4 \cdot 2H_2O$, Figure 1) by the Brust method.[44] After synthesis, MCGNPs were mixed with additives and manually drop-casted onto an electrode surface to form a sensor. Finalization of the sensor was achieved after additive removal via a washout procedure and subsequent annealing. Sensor and MCGNP characterization was performed using SEM, ATR, and TEM analysis as well as pure-gas exposure tests.

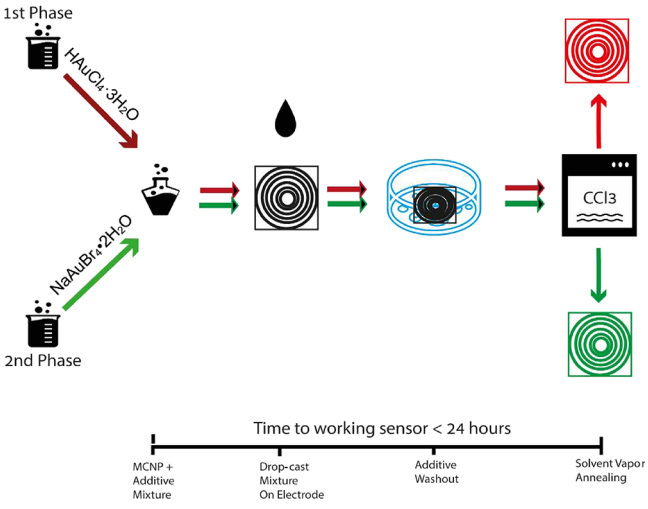

Figure 1. Schematic of the MCGNP-based sensor fabrication process using either $HAuCl_4 \cdot 3H_2O$ or $NaAuBr_4 \cdot 2H_2O$ as the gold precursor.

Surface Characterization of Additive-Supplemented $HAuCl_4 \cdot 3H_2O$-Based MCGNP Films. Each step of the fabrication process was monitored by SEM and ATR. SEM analysis reveals that drop-casting of MCGNPs on top of the electrode surface results in MCGNP congestion and the formation of coffee ring structures at the naïve drop periphery (Figure 2a). This nonuniformity on the sensor surface had been previously suggested to result in low reproducibility.[33,45,46] On the other hand, these coffee ring structures were absent in the additive-supported sensor, which showed improved dispersion on the electrode surface where spheres

https://doi.org/10.1021/acsomega.2c01668
ACS Omega 2022, 7, 22484−22491

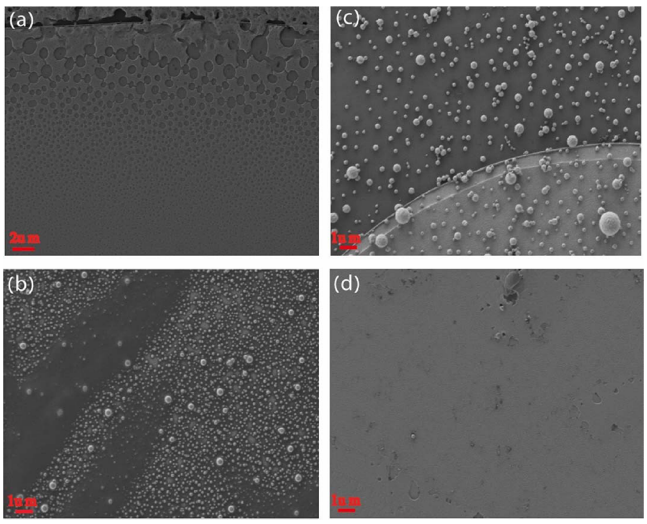

Figure 2. Representative SEM images of MCGNPs drop-casted with or without additives. (a) Naïve MCGNPs forming coffee ring structures on the periphery of the droplet. (b) Additive-supplemented MCGNPs. (c) Additive-supplemented MCGNPs postwashing. (d) Additive-supplemented MCGNPs postannealing (higher-magnification images are provided in Supporting Information, Figure S1). The scale size is present on each image.

cover the entire field of view (Figure 2b). This dispersion pattern was still present after washing, although fewer spheres are visible, explained by partial particle removal due to the washing step (Figure 2c). Preannealing, the MCGNPs are visible as small spheres (single or grouped nanoparticles), and after solvent vapor annealing (SVA), the spheres form a connected network that looks like a "smeared paste" on top of the electrode surface (Figure 2d). This is consistent with the SVA phenomena previously described in the literature.[42]

ATR can identify the chemical bonds of interest and therefore was used in this study to confirm the additive removal and the MCGNP ligand integrity. Naïve or additive-supplemented MCGNPs drop-casted on a cleaned silicon wafer confirmed the correct identification of the thiolated ligand, which is marked with a red arrow at approximately 2900 nm (Figure 3). This band was not visible in an additive-only-containing silicon wafer (Figure 3c) when compared with an MCGNP-containing silicon wafer (Figure 3a,b). In addition, two more visible bands are seen at values below 2900 nm. However, they are seen even when MCGNPs or additives are not present and therefore are not relevant either (Figure 3a−c). The ligand is still visible even after the MCGNP-containing silicon wafer is submerged in a washing solution for 2h and subsequently annealed (Figure 3d,e), indicating that the ligand is undamaged and sufficient particles are still present on the surface. Additive removal was confirmed by identifying the additive-relevant bands at the 1300−1700 nm range. The composition is unknown of the patent-protected additives, so we searched for bands that are mutual in an additive-containing silicon wafer but absent when additives are absent (Figure 3f, red and green lines versus black line). Detection of materials in these wavelengths indicated that additives are present on the silicon surface. Indeed, we failed to obtain a signal at those wavelengths after washing or annealing (Figure 3f, purple and blue lines, respectively), suggesting full removal of the additives.

Controlled MCGNP Synthesis Using $NaAuBr_4 \cdot 2H_2O$. Recently, Booth *et al.* showed that MCGNPs synthesized through the Brust method using $HAuCl_4 \cdot 3H_2O$ have a tendency to form an unstable active gold component that results in the formation of agglomerates during the synthesis step.[40] These agglomerates are composed of thousands or perhaps millions of individual nanoparticles. Agglomeration results in two individually sized MCGNP populations. A sensor composed of such MCGNPs is expected to be faulty or with a reduced shelf life at best. The inability to control large particle positions on the sensing layer can result in sensor variability. In addition, large particle localization can influence the electron transport via reduced output,[47] and agglomerated particles can be vulnerable to humidity, oxidization, heat, and other environmental cues. Particle agglomeration also increases the sensor recovery time.[48,49] With this in mind, we have used $NaAuBr_4 \cdot 2H_2O$ as a precursor for MCGNP synthesis,[40] to avoid agglomeration. Confirmation of the results was visually obtained with TEM analysis (Figure 4a,b), which showed lack of agglomeration in $NaAuBr_4 \cdot 2H_2O$ and the existence of agglomeration in $HAuCl_4 \cdot 3H_2O$-based solutions. Specifically, nonagglomerated particles appear as single particles with no halo (Figure 4a). Meanwhile, agglomerated particles form a halo around them due to their size when injected on the TEM carbon membrane (Figure 4b). Switching the precursor to bromide from chloride has no detrimental effect on the particle diameter as shown via particle size histograms (Figure 4c,d).

Sensor Fabrication of Additive-Supplemented $HAuCl_4 \cdot 3H_2O$-Based MCGNPs. This method produces drop-casted thin-film MCGNPs where coffee ring formation is inhibited. This method allows improved cover utilization of the electrode surface. This improved cover yields a sensor with reproducible performance when exposed to gas (Figure 5a,b showing five replicate sensors, each marked by a different color). Reproducibility was demonstrated with the sensor signals almost situated on top of each other (Figure 5a,b), which produced features with low standard deviation when exposed to *p*-xylene at different concentrations (Figure 5d). Furthermore, the signal produced is "clean" with a high signal to noise ratio when exposed to a pure gas such as hexanol at 0−80 ppm (Figure 5a) or 1,2,4-trimethylbenzene (TMB) at 0−80 ppm (Figure 5b) or *p*-xylene at 20 ppm (Figure 5c). The sensor performance can be attributed to the annealing step stabilizing the MCGNPs on the electrode surface forming thermodynamically favorable interactions (Figure 2d versus Figure 2b).[42] On the other hand, the lack of additive usage in the fabrication results in a nonhomogeneous electrode MCGNP cover and coffee ring formation. When exposed, such sensors produce a noisy signal output (Figure 6a,b), demonstrating a low signal to noise ratio. Sensors produced in this manner are nonreproducible due to the uncontrolled particle deposition on the electrode surface and suffer from low performance. Specifically, such sensors cannot discriminate between different concentrations of a hexanol pure gas at 40 ppm versus 20 ppm (Figure 6a) or a TMB pure gas at 80 ppm versus 40 ppm (Figure 6b). They also cannot discriminate between a hexanol pure gas and a TMB pure gas since at 20 ppm, they provide a similar delta in resistance (Figure 6a,b). It was found that the addition of additives without their removal results in increased resistance changes when exposed to gas. However, this produces additional noise (Figure 6c) resulting in high sensor variance within batches and prevents reproducibility. This is demonstrated by features extracted

https://doi.org/10.1021/acsomega.2c01668
ACS Omega 2022, 7, 22484−22491

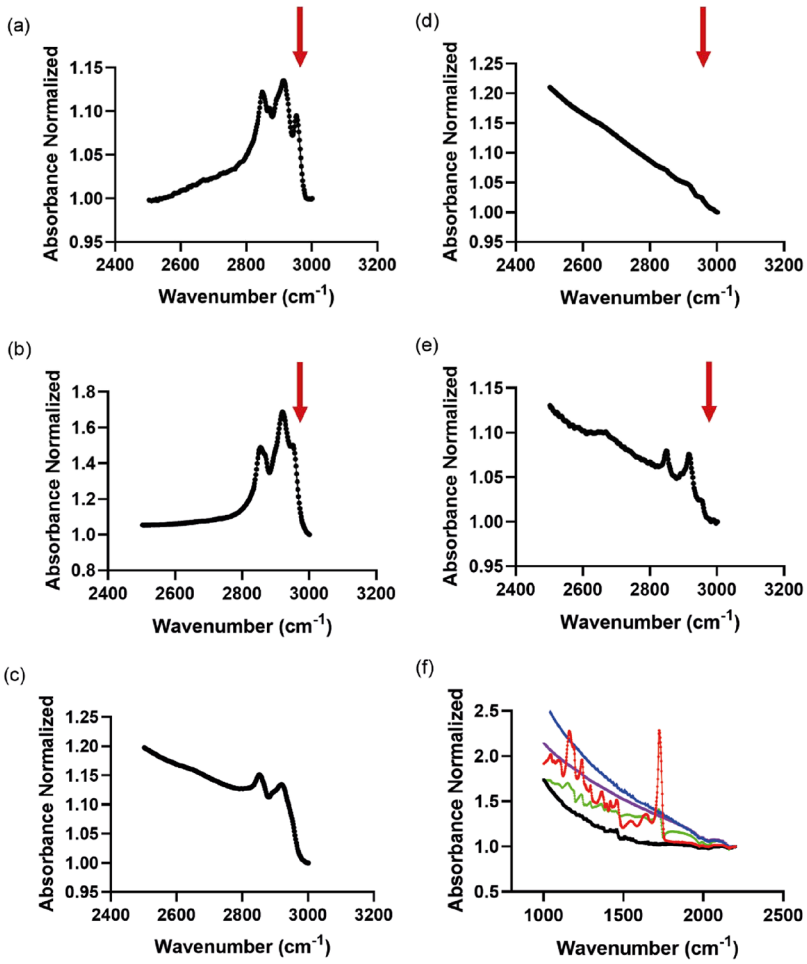

Figure 3. Representative ATR surface characterization of deposited MCGNPs. (a) Naïve MCGNPs. (b) Additive-supplemented MCGNPs. (c) Additives only. (d) Additive-supplemented MCGNPs postwashing. (e) Additive-supplemented MCGNPs after washing and annealing. (f) Step by step follow-up on additive removal, (black line) naïve MCGNPs, (green line) additives only, (red line) additives and MCGNPs, (purple line) washed supplemented MCGNPs, and (blue line) washed and annealed supplemented MCGNPs. Arrows point at the ligand-associated peak of MCGNPs.

from such sensors with high standard deviation when exposed to *p*-xylene (Figure 6d). To be noted, the inversion of the response in both Figures 5d and 6d was investigated in a previous study by Tisch and Haick.[23] To further support this technique, we have synthesized MCGNPs with different capping agents (i.e., different ligands) and exposed the fabricated sensors to TMB and hexanol in different concentrations obtaining the same clean and reproducible signal (see Supporting Information, Figure S2 and Table S1).

The link between the improved cover of the nanoparticle dispersion on sensor signal reproducibility can be explained by the electron transfer on the electrode surface during exposure. Naturally, electrical current will pass through the least resistive route. The coffee ring milieu is a high-density environment of particles, and therefore, the resistance throughout the coffee ring structure is smaller than the resistance in other parts of the electrode that are less occupied by nanoparticles, where the interparticle distance is enlarged and substantially more affected by the particles' ligand to ligand orientation. In essence, electrical current in coffee ring-containing devices is more prone to signal instability. Comparably, in higher-percolation thin films, the electrical current can move through various routes (similar to electrons passing from the anode to the cathode), and the complete electrode surface is efficiently utilized.[23,50,51] This is shown macroscopically in Figure S3 in the Supporting Information where the coffee ring can be seen in the naïve sensors, whereas it is nonvisible in the additive-supported sensors. This figure also shows the reproducibility of the latter over the former where the density in the coffee ring compared with the center is hard to control.

Fabrication of a $NaAuBr_4 \cdot 2H_2O$-Based Tunable MCGNP Sensor with Desired Characteristics. The use of the above-described additives for fabrication of a thin-layer MCGNP and the combination with the improved MCGNP synthesis protocol produced a tunable sensor. By modifying the particle ligand ratio, it was shown that the intrinsic sensing characteristics of these particles can be tailor-made and controlled. A sensor synthesized with a 0.5 S:Au ratio can discriminate a pure gas in 20 ppm concentration intervals, while a 1.5 ratio results in inaccurate measurements. This can be seen on the response curve (Figure 7a) and the feature values with variance in Figure 7b,c, respectively. Lowering the ligand:gold ratio formed sensors with significantly lower baseline resistance (indicating that a lower interparticle spacing due to a reduced particle ligand cover is the dominant force and not the increased particle size[52]). Thus, the 0.5 S:Au ratio sensor with superior performance could be the result of flexible ligand orientation and mobility.[53] Either way, $NaAuBr_4 \cdot 2H_2O$-

https://doi.org/10.1021/acsomega.2c01668
ACS Omega 2022, 7, 22484−22491

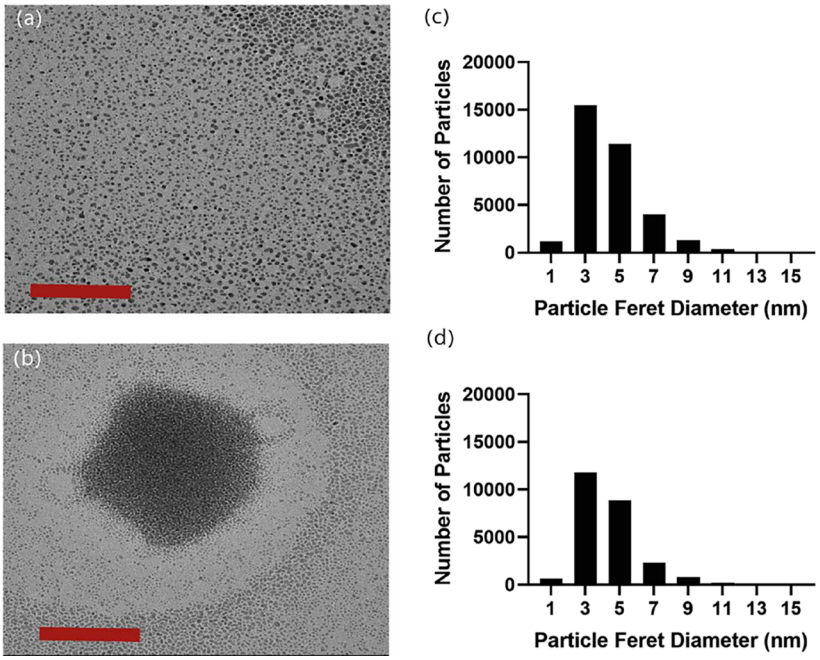

Figure 4. Synthesis of *tert*-dodecanethiol gold nanoparticles using $HAuCl_4 \cdot 3H_2O$ and $NaAuBr_4 \cdot 2H_2O$. TEM imaging of (a) $NaAuBr_4 \cdot 2H_2O$ and (b) $HAuCl_4 \cdot 3H_2O$; the scale of 100 nm shows visually the difference between particle sizes. Size histograms of respective particles of (c) $NaAuBr_4 \cdot 2H_2O$ and (d) $HAuCl_4 \cdot 3H_2O$ showing similar particle size when excluding agglomerated particles. Both MCGNPs were synthesized using similar S:Au ratios (1.5).

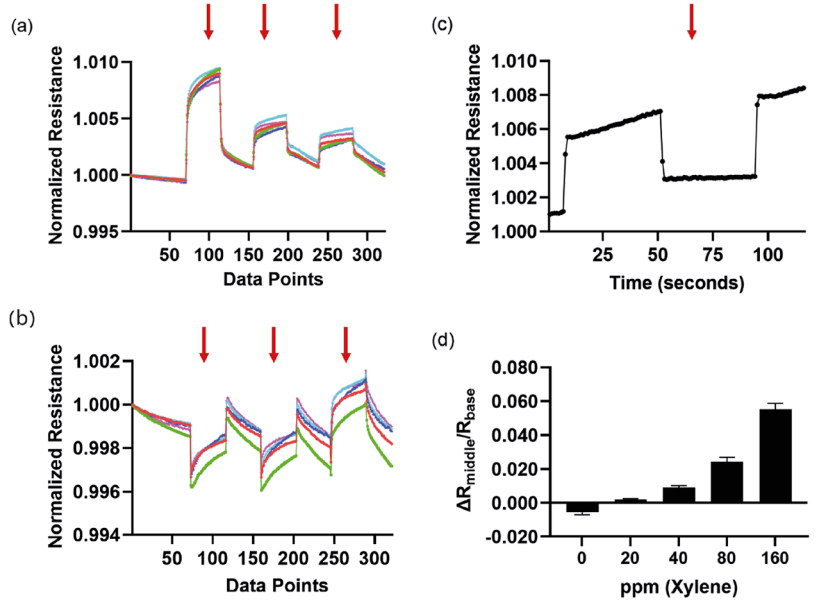

Figure 5. Additive-supplemented MCGNP-based sensors. (a) Five sensors after additive removal and postannealing exposed to a hexanol pure gas (80, 40, and 20 ppm, arrows from left to right) (b) and a TMB pure gas (80, 40, and 20 ppm, arrows from left to right). (c) Sensor response to 20 ppm *p*-xylene after additive removal and annealing. The arrow points at the time of gas exposure; data points represent 5s intervals. (d) Feature value (mean ± SD) of postannealing response of the measured five sensors exposed to *p*-xylene.

based MCGNPs offer advantages in the form of a homogeneous size and shape of these particles resulting in a sensor that is more efficient in electron transfer and possibly resistant to environmental insults (due to particle redundancy[54] or reduced organic layer thickness).

SUMMARY AND CONCLUSIONS

Most laboratory work that develops new sensors and the surrounding work encounter difficulties such as the irreproducibility of sensor performance, often leading to biased results, faulty conclusions, and wastage of raw materials. The sensors presented in this report are easily reproduced, and the surfactants used are simple to remove, guaranteeing pure, direct interactions of the target analyte with the MCGNPs. The results suggest that sensors produced via this method have an increased limit of detection, differentiation, and stability quality. The fabrication method is specifically aimed for laboratory research purposes but can be quickly adapted to

https://doi.org/10.1021/acsomega.2c01668
ACS Omega 2022, 7, 22484−22491

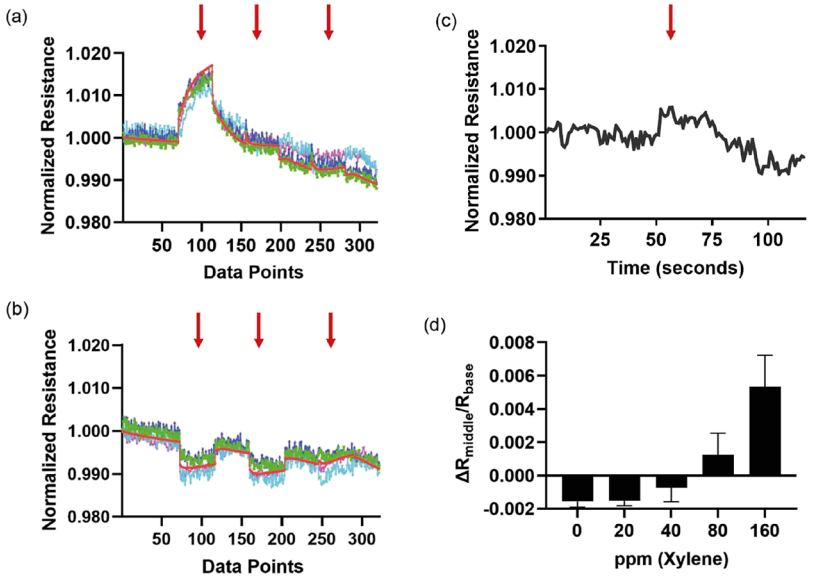

Figure 6. Naïve sensors produced using MCGNPs. (a) Five sensors exposed to a hexanol pure gas (80, 40, and 20 ppm, arrows from left to right). (b) Five sensors exposed to a TMB pure gas (80, 40, and 20 ppm, arrows from left to right). (c) Sensor response to 20 ppm *p*-xylene without additive removal. The arrow points at the time of gas exposure; data points represent 5s intervals. (d) Feature value (mean ± SD) of five measured naïve sensors exposed to *p*-xylene.

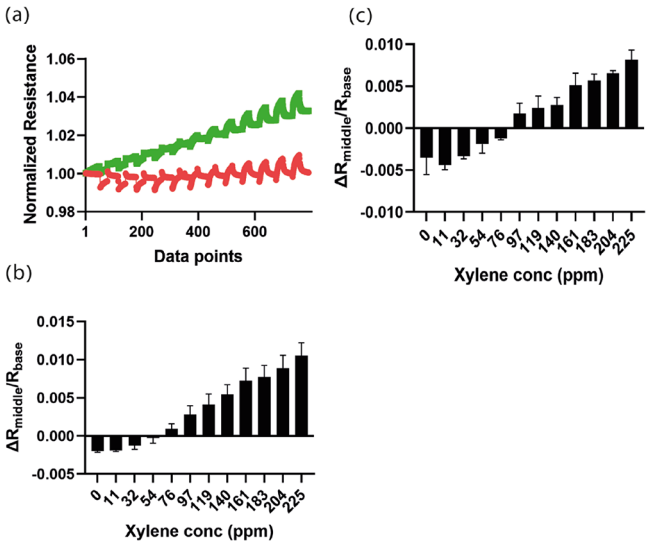

Figure 7. Tailor-made sensor using different concentrations of the thiol ligand. (a) Sensor resistance measured in response to an *m*-xylene pure gas at 20 ppm intervals (0−225 ppm); data points represent 5s intervals for different S:Au ratios (1.5 S:Au (red), 0.5 S:Au (green)). (b) Resistance delta of three sensors (0.5 S:Au ratio) exposed to 20 ppm intervals of *m*-xylene (0−225 ppm) (mean ± SD). (c) Feature value of three sensors (1.5 S:Au ratio) exposed to 20 ppm intervals of *m*-xylene (0−225 ppm) (mean ± SD).

scaled-up production of such sensors. The described method can also be adapted to produce other thiol ligand and metal-based nanoparticles on rigid or flexible surfaces.

■ ASSOCIATED CONTENT

Supporting Information

The Supporting Information is available free of charge at https://pubs.acs.org/doi/10.1021/acsomega.2c01668.

(Figure S1) Magnification of Figure 2d, (Figure S2) sensors produced via the described method using different ligands, (Table S1) detailed identification of the additional ligands used, and (Figure S3) macroscopic visualization of the electrode surface postnanoparticle casting (PDF)

■ AUTHOR INFORMATION

Corresponding Author

Hossam Haick − *The Department of Chemical Engineering and The Russell Berrie Nanotechnology Institute, Technion − Israel Institute of Technology, Haifa 3200003, Israel;* orcid.org/0000-0002-2370-4073; Email: hhossam@technion.ac.il

Authors

Elias Mansour − *The Department of Chemical Engineering, Technion − Israel Institute of Technology, Haifa 3200003, Israel*

Shay Sherbo − *The Department of Chemical Engineering, Technion − Israel Institute of Technology, Haifa 3200003, Israel*

Walaa Saliba − *The Department of Chemical Engineering, Technion − Israel Institute of Technology, Haifa 3200003, Israel*

Viki Kloper − *The Department of Chemical Engineering, Technion − Israel Institute of Technology, Haifa 3200003, Israel*

Complete contact information is available at: https://pubs.acs.org/10.1021/acsomega.2c01668

Author Contributions

§E.M. and S.S. contributed equally to this work.

Notes

The authors declare no competing financial interest.

https://doi.org/10.1021/acsomega.2c01668
ACS Omega 2022, 7, 22484−22491

■ ACKNOWLEDGMENTS

The authors hereby acknowledge the help of Nitai Arbell and Dorit Greenberg from the lab of Prof. Yaron Paz in the Department of Chemical Engineering, Technion.

■ REFERENCES

(1) Vishinkin, R.; Busool, R.; Mansour, E.; Fish, F.; Esmail, A.; Kumar, P.; Gharaa, A.; Cancilla, J. C.; Torrecilla, J. S.; Skenders, G.; Leja, M.; Dheda, K.; Singh, S.; Haick, H. Profiles of Volatile Biomarkers Detect Tuberculosis from Skin. *Adv. Sci.* **2021**, *8*, 2100235.

(2) Broza, Y. Y.; Kremer, R.; Tisch, U.; Gevorkyan, A.; Shiban, A.; Best, L. A.; Haick, H. A Nanomaterial-Based Breath Test for Short-Term Follow-up after Lung Tumor Resection. *Nanomed. Nanotechnol., Biol. Med.* **2013**, *9*, 15−21.

(3) Peng, G.; Hakim, M.; Broza, Y. Y.; Billan, S.; Abdah-Bortnyak, R.; Kuten, A.; Tisch, U.; Haick, H. Detection of Lung, Breast, Colorectal and Prostate Cancers from Exhaled Breath Using a Single Array of Nanosensors. *Br. J. Cancer* **2010**, *103*, 542−551.

(4) Nakhleh, M. K.; Amal, H.; Jeries, R.; Broza, Y. Y.; Aboud, M.; Gharra, A.; Ivgi, H.; Khatib, S.; Badarneh, S.; Har-Shai, L.; Glass-Marmor, L.; Lejbkowicz, I.; Miller, A.; Badarny, S.; Winer, R.; Finberg, J.; Cohen-Kaminsky, S.; Perros, F.; Montani, D.; Girerd, B.; Garcia, G.; Simonneau, G.; Nakhoul, F.; Baram, S.; Salim, R.; Hakim, M.; Gruber, M.; Ronen, O.; Marshak, T.; Doweck, I.; Nativ, O.; Bahouth, Z.; Shi, D. Y.; Zhang, W.; Hua, Q. L.; Pan, Y. Y.; Tao, L.; Liu, H.; Karban, A.; Koifman, E.; Rainis, T.; Skapars, R.; Sivins, A.; Ancans, G.; Liepniece-Karele, I.; Kikuste, I.; Lasina, I.; Tolmanis, I.; Johnson, D.; Millstone, S. Z.; Fulton, J.; Wells, J. W.; Wilf, L. H.; Humbert, M.; Leja, M.; Peled, N.; Haick, H. Diagnosis and Classification of 17 Diseases from 1404 Subjects via Pattern Analysis of Exhaled Molecules. *ACS Nano* **2017**, *11*, 112−125.

(5) Broza, Y. Y.; Zuri, L.; Haick, H. Combined Volatolomics for Monitoring of Human Body Chemistry. *Sci. Rep.* **2015**, *4*, 4611.

(6) Marć, M.; Zabiegała, B.; Namieśnik, J. Testing and Sampling Devices for Monitoring Volatile and Semi-Volatile Organic Compounds in Indoor Air. *TrAC - Trends Anal. Chem.* **2012**, *32*, 76−86.

(7) Zhang, H.; Srinivasan, R. A Systematic Review of Air Quality Sensors, Guidelines, and Measurement Studies for Indoor Air Quality Management. *Sustainability* **2020**, 1−40. Multidisciplinary Digital Publishing Institute October 30

(8) Szulczyński, B.; Gębicki, J. Currently Commercially Available Chemical Sensors Employed for Detection of Volatile Organic Compounds in Outdoor and Indoor Air. *Environ. MDPI* **2017**, *4*, 1−15.

(9) Tiwari, S.; Kate, A.; Mohapatra, D.; Tripathi, M. K.; Ray, H.; Akuli, A.; Ghosh, A.; Modhera, B. Volatile Organic Compounds (VOCs): Biomarkers for Quality Management of Horticultural Commodities during Storage through e-Sensing. *Trends Food Sci. Technol.* **2020**, *106*, 417−433.

(10) Loutfi, A.; Coradeschi, S.; Mani, G. K.; Shankar, P.; Rayappan, J. B. B. Electronic Noses for Food Quality: A Review. *J. Food Eng.* **2015**, *144*, 103−111.

(11) Lytou, A. E.; Panagou, E. Z.; Nychas, G. J. E. Volatilomics for Food Quality and Authentication. *Curr. Opin. Food Sci.* **2019**, *28*, 88−95.

(12) Vishinkin, R.; Haick, H. Nanoscale Sensor Technologies for Disease Detection via Volatolomics. *Small* **2015**, 6142−6164. John Wiley & Sons, Ltd December 1

(13) Broza, Y. Y.; Vishinkin, R.; Barash, O.; Nakhleh, M. K.; Haick, H. Synergy between Nanomaterials and Volatile Organic Compounds for Non-Invasive Medical Evaluation. *Chem. Soc. Rev.* **2018**, *47*, 4781−4859. Royal Society of Chemistry July

(14) Hu, W.; Wan, L.; Jian, Y.; Ren, C.; Jin, K.; Su, X.; Bai, X.; Haick, H.; Yao, M.; Wu, W. Electronic Noses: From Advanced Materials to Sensors Aided with Data Processing. *Adv. Mater. Technol.* **2019**, 1800488. John Wiley & Sons, Ltd February 1

(15) Konvalina, G.; Haick, H. Sensors for Breath Testing: From Nanomaterials to Comprehensive Disease Detection. *Acc. Chem. Res.* **2014**, 66.

(16) Dovgolevsky, E.; Tisch, U.; Haick, H. Chemically Sensitive Resistors Based on Monolayercapped Cubic Nanoparticles: Towards Configurable Nanoporous Sensors. *Small* **2009**, *5*, 1158−1161.

(17) Segev-Bar, M.; Shuster, G.; Haick, H. Effect of Perforation on the Sensing Properties of Monolayer-Capped Metallic Nanoparticle Films. *J. Phys. Chem. C* **2012**, *116*, 15361−15368.

(18) Chow, E.; Raguse, B.; Müller, K. H.; Wieczorek, L.; Bendavid, A.; Cooper, J. S.; Hubble, L. J.; Webster, M. S. Influence of Gold Nanoparticle Film Porosity on the Chemiresistive Sensing Performance. *Electroanalysis* **2013**, *25*, 2313−2320.

(19) Brust, M.; Walker, M.; Bethell, D.; Schiffrin, D. J.; Whyman, R. Synthesis of Thiol-Derivatised Gold Nanoparticles in a Two-Phase Liquid-Liquid System. *J. Chem. Soc., Chem. Commun.* **1994**, *7*, 801−802.

(20) Jana, N. R.; Peng, X. Single-Phase and Gram-Scale Routes toward Nearly Monodisperse Au and Other Noble Metal Nanocrystals. *J. Am. Chem. Soc.* **2003**, *125*, 14280−14281.

(21) Martin, M. N.; Basham, J. I.; Chando, P.; Eah, S. K. Charged Gold Nanoparticles in Non-Polar Solvents: 10-Min Synthesis and 2D Self-Assembly. *Langmuir* **2010**, *26*, 7410−7417.

(22) Sau, T. K.; Murphy, C. J. Room Temperature, High-Yield Synthesis of Multiple Shapes of Gold Nanoparticles in Aqueous Solution. *J. Am. Chem. Soc.* **2004**, *126*, 8648−8649.

(23) Tisch, U.; Haick, H. Arrays of Chemisensitive Monolayer-Capped Metallic Nanoparticles for Diagnostic Breath Testing. *Rev. Chem. Eng.* **2011**, *1*, 171−179.

(24) Ram, M. K.; Yavuz, Ö.; Lahsangah, V.; Aldissi, M. CO Gas Sensing from Ultrathin Nano-Composite Conducting Polymer Film. *Sens. Actuators, B* **2005**, *106*, 750−757.

(25) Bashouti, M. Y.; De La Zerda, A. S.; Geva, D.; Haick, H. Designing Thin Film-Capped Metallic Nanoparticles Configurations for Sensing Applications. *J. Phys. Chem. C* **2014**, *118*, 1903−1909.

(26) Chern, G. C.; Lauks, I. Spin-Coated Amorphous Chalcogenide Films. *J. Appl. Phys.* **1982**, *53*, 6979−6982.

(27) Perednis, D.; Gauckler, L. J. Thin Film Deposition Using Spray Pyrolysis. *J. Electroceram.* **2005**, *14*, 103−111.

(28) Kaliyaraj Selva Kumar, A.; Zhang, Y.; Li, D.; Compton, R. G. A Mini-Review: How Reliable Is the Drop Casting Technique? *Electrochem. Commun.* **2020**, No. 106867.

(29) Mampallil, D.; Eral, H. B. A Review on Suppression and Utilization of the Coffee-Ring Effect. *Adv. Colloid Interface Sci.* **2018**, *252*, 38−54.

(30) Zang, D.; Tarafdar, S.; Tarasevich, Y. Y.; Dutta Choudhury, M.; Dutta, T. Evaporation of a Droplet: From Physics to Applications. *Phys. Rep.* **2019**, *804*, 1−56.

(31) Han, W.; Lin, Z. Learning from "Coffee Rings:" Ordered Structures Enabled by Controlled Evaporative Self-Assembly. *Angew. Chem., Int. Ed.* **2012**, *51*, 1534−1546.

(32) Araki, K.; Mizuguchi, E.; Tanaka, H.; Ogawa, T. Preparation of Very Reactive Thiol-Protected Gold Ianoparticles: Revisiting the Brust-Schiffrin Method. *J. Nanosci. Nanotechnol.* **2006**, *6*, 708−712.

(33) Patil, N. D.; Bhardwaj, R. Recent Developments on Colloidal Deposits Obtained by Evaporation of Sessile Droplets on a Solid Surface. *J. Indian Inst. Sci.* **2019**, *99*, 143−156.

(34) Pesach, D.; Marmur, A. Marangoni Effects in the Spreading of Liquid Mixtures on a Solid. *Langmuir* **1987**, *3*, 519−524.

(35) Bekki, S.; Vignes-Adler, M.; Nakache, E.; Adler, P. M. Solutal Marangoni Effect. I. Pure Interfacial Transfer. *J. Colloid Interface Sci.* **1990**, *140*, 492−506.

(36) Anyfantakis, M.; Geng, Z.; Morel, M.; Rudiuk, S.; Baigl, D. Modulation of the Coffee-Ring Effect in Particle/Surfactant Mixtures: The Importance of Particle-Interface Interactions. *Langmuir* **2015**, *31*, 4113−4120.

(37) Hu, H.; Larson, R. G. Marangoni Effect Reverses Coffee-Ring Depositions. *J. Phys. Chem. B* **2006**, *110*, 7090−7094.

https://doi.org/10.1021/acsomega.2c01668
ACS Omega 2022, 7, 22484−22491

(38) Mugele, F.; Baret, J. C. Electrowetting: From Basics to Applications. *J. Phys.: Condens. Matter* **2005**, *17*, R705. IOP Publishing July
(39) Schneider, D.; Schwarz, T.; Bradford, A. S.; Shan, Q.; Dewhurst, R. J. Controlling the Quality of Thin Films by Surface Acoustic Waves. *Ultrasonics* **1997**, *35*, 345−356.
(40) Booth, S. G.; Uehara, A.; Chang, S. Y.; La Fontaine, C.; Fujii, T.; Okamoto, Y.; Imai, T.; Schroeder, S. L. M.; Dryfe, R. A. W. The Significance of Bromide in the Brust-Schiffrin Synthesis of Thiol Protected Gold Nanoparticles. *Chem. Sci.* **2017**, 7954.
(41) Milyutin, Y.; Abud-Hawa, M.; Kloper-Weidenfeld, V.; Mansour, E.; Broza, Y. Y.; Shani, G.; Haick, H. Fabricating and Printing Chemiresistors Based on Monolayer-Capped Metal Nanoparticles. *Nat. Protoc.* **2021**, 2968.
(42) De Luca, G.; Treossi, E.; Liscio, A.; Mativetsky, J. M.; Scolaro, L. M.; Palermo, V.; Samorí, P. Solvent Vapour Annealing of Organic Thin Films: Controlling the Self-Assembly of Functional Systems across Multiple Length Scales. *J. Mater. Chem.* **2010**, 2493.
(43) Riedel, L. Eine Neue Universelle Dampfdruckformel Untersuchungen Über Eine Erweiterung Des Theorems Der Übereinstimmenden Zustände. Teil I. *Chem. Ing. Technol.* **1954**, *26*, 83−89.
(44) Uehara, A.; Booth, S. G.; Chang, S. Y.; Schroeder, S. L. M.; Imai, T.; Hashimoto, T.; Mosselmans, J. F. W.; Dryfe, R. A. W. Electrochemical Insight into the Brust-Schiffrin Synthesis of Au Nanoparticles. *J. Am. Chem. Soc.* **2015**, *137*, 15135−15144.
(45) Azoubel, S.; Shemesh, S.; Magdassi, S. Flexible Electroluminescent Device with Inkjet-Printed Carbon Nanotube Electrodes. *Nanotechnology* **2012**, *23*, No. 344003.
(46) Theerthagiri, J.; Lee, S. J.; Karuppasamy, K.; Park, J.; Yu, Y.; Kumari, M. L. A.; Chandrasekaran, S.; Kim, H. S.; Choi, M. Y. Fabrication Strategies and Surface Tuning of Hierarchical Gold Nanostructures for Electrochemical Detection and Removal of Toxic Pollutants. *J. Hazard. Mater.* **2021**, *420*, No. 126648.
(47) Altmann, L.; Sturm, H.; Brauns, E.; Lang, W.; Bäumer, M. Novel Catalytic Gas Sensors Based on Functionalized Nanoparticle Layers. *Sens. Actuators, B* **2012**, *174*, 145−152.
(48) Lee, J. H. Gas Sensors Using Hierarchical and Hollow Oxide Nanostructures: Overview. *Sens. Actuators, B* **2009**, *140*, 319−336.
(49) Kim, H. R.; Choi, K. I.; Lee, J. H.; Akbar, S. A. Highly Sensitive and Ultra-Fast Responding Gas Sensors Using Self-Assembled Hierarchical SnO2 Spheres. *Sens. Actuators, B* **2009**, *136*, 138−143.
(50) Ibañez, F. J.; Zamborini, F. P. Chemiresistive Sensing with Chemically Modified Metal and Alloy Nanoparticles. *Small* **2012**, 174−202. John Wiley & Sons, Ltd January 23
(51) Montes-Garcia, V.; Squillaci, M. A.; Diez-Castellnou, M.; Ong, Q. K.; Stellacci, F.; Samorí, P. Chemical Sensing with Au and Ag Nanoparticles. *Chem. Soc. Rev.* **2021**, *50*, 1269−1304. Royal Society of Chemistry February
(52) Haick, H. Chemical Sensors Based on Molecularly Modified Metallic Nanoparticles. *J. Phys. D: Appl. Phys.* **2007**, *40*, 7173−7186.
(53) Salorinne, K.; Malola, S.; Wong, O. A.; Rithner, C. D.; Chen, X.; Ackerson, C. J.; Häkkinen, H. Conformation and Dynamics of the Ligand Shell of a Water-Soluble Au 102 Nanoparticle. *Nat. Commun.* **2016**, *7*, 1.
(54) Barfidokht, A.; Ciampi, S.; Luais, E.; Darwish, N.; Gooding, J. J. Distance-Dependent Electron Transfer at Passivated Electrodes Decorated by Gold Nanoparticles. *Anal. Chem.* **2013**, *85*, 1073−1080.

https://doi.org/10.1021/acsomega.2c01668
ACS Omega 2022, 7, 22484−22491